Stirring: The Eckart paradigm revisited

Stirring: The Eckart Paradigm Revisited

M. Branicki, A. D. Kirwan, Jr.

College of Earth, Ocean, and Environment, Robinson Hall, University of Delaware, Newark DE 19716 USA

Abstract

This report provides a topical review of transport in geophysical scale fluids. Rather than presenting an extensive synopsis of the literature, we attempt to connect some recent developments with an incisive 1948 paper by Carl Eckart [1] in which three phases in the evolution of a tracer in turbulent flows were outlined and discussed. The interest here is on the intermediate or *stirring* phase, which is dominated by the fluid deformation rate. We relate Eckart's concept of stirring with recent efforts to identify ephemeral spatio-temporal channels that provide a template for transport in geophysical fluid flows. Heretofore such studies have been restricted to a few selected surfaces in the ocean or atmosphere. An application to a large ocean eddy in the Gulf of Mexico illustrates the methodology and shows that the eddy exchanges mass with its environment through material channels identified in the Lagrangian frame by finite-time dynamical systems techniques. We extend previous studies by determining the vertical extent of these transport pathways. The key finding is that the time-dependent geometric structures, which lead to formation of these pathways, retain their coherence well into the water column. Finally, we comment on the significance of these findings on parameterizations of transport processes in predictive models and on the life cycle of ocean mesoscale eddies.

Keywords: Hyperbolic trajectories, stirring, time-dependent transport, stable and unstable manifolds, Lyapunov exponents, 3D ocean eddies

1. Introduction

The notion of fluid stirring originated with Carl Eckart's [1] casual observation of motions induced by pouring cream into a cup of coffee. The swirling

motions in his cup motivated him to derive evolution equations for the variance of the gradient of a passive scalar, i.e. cream. Eckart identified three phases in the evolution of the mixture of cream and coffee. During the initial phase, the cream and coffee regimes are only mildly distorted from their initial distributions. Although the concentration gradient of the cream contains sharp fronts, the variance of the gradient averaged over the cup is small. The intermediate, or stirring, phase is characterized by huge distortions of the cream accompanied by the development of small-scale structures (relative to the characteristic length scale of the initial distribution) commonly referred to as fingers, swirls, and squirts. At this stage, the concentration gradients still contain sharp fronts but their variance is larger than in the initial stage, owing to the convoluted geometry of the cream patch, which is now spread over a large portion of the coffee cup. The final stage occurs when molecular diffusion dominates, the strong gradients disappear, and the system approaches a desired homogeneous state.

Although Eckart's model was motivated by mixing of cream in coffee, his subsequent discussion focused on application to geophysical scales in the ocean and atmosphere. His analysis raises two fundamental issues. The first is: stirring is an ubiquitous phenomenon that often occurs in flows on scales larger than the Kolmogorov or diffusive length scales. Second, transport processes in such flows, traditionally treated by statistical means whereby the fluxes are parameterized as eddy diffusivities, are actually deterministic intense small-scale advective events.

Eckart's paper has received widespread genuflection, particularly from the geophysical fluid dynamics community, see [2] for example. Nevertheless most researchers still adhere to eddy diffusivity models to parameterize stirring processes. However, a number of workers have started to apply ideas from dynamical systems theory to study advective processes at stirring scales. Wiggins [3] has provided a recent and extensive review of this work. It is ironic that insight arising from this geometric approach, originally motivated by Lorenz's [4] famous analysis of a convective geophysical scale flow, is not yet used by the geophysical fluid dynamics community to construct better parameterizations for stirring type processes.

A primary goal here is to show that Eckart [1] anticipated much later applications of dynamical systems theory to advection-dominated transport in fluids. His analysis suggested that an important phase of processes ranging from the stirring of cream in a coffee cup to mesoscale phenomena such as eddies, squirts, and jets seen in the ocean and atmosphere can be un-

derstood in geometric terms of the quasi-conservative evolution of material tracer contours. Moreover, he deduced that the fluid deformation rate, not the vorticity, is the critical diagnostic during the second phase of his tracer evolution scenario. This may appear to be counterintuitive to some since vortical motions associated with eddies typically dominate such flows.

Our view is that dynamical systems theory provides a useful template for determining Lagrangian, spatio-temporal properties of flows at scales where advection is dominant. A key issue is to locate and focus on certain *hyperbolic* fluid parcel trajectories, which can be loosely thought of as moving saddle-points. A more detailed discussion of these matters is deferred to section 3. These ephemeral trajectories typically live in the unsteady nether regions between eddies. They are found at the intersection of special material manifolds that delineate the small-scale structures in Eckart's description of stirring, i.e. scales which are small relative to the characteristic length of the initial tracer distribution yet large compared to the diffusive length scales. Curiously, the hyperbolic regions between the eddies are characterized by small velocities, yet they are often the regions associated with the largest distortion. The deformation rate there may be an order of magnitude larger than the vorticity.

Previous applications of dynamical systems theory to fluid dynamics and particularly geophysical fluid dynamics are nearly always restricted to two-dimensional analysis along isentropic, isopycnal or simply horizontal surfaces (see, for example, [5, 6, 7, 8, 9, 10, 11]). Moreover, oceanic applications are generally confined to the near-surface flows. Of course real geophysical fluid flows may vary significantly in the vertical. The hyperbolic trajectories and their stable and unstable manifolds identified by 2D analyses of 3D flow fields provide, at best, information about intersections of some higher-dimensional structures with the 2D surfaces. In stratified flows, curves obtained by vertically stacking instantaneous locations of the 2D hyperbolic trajectories, identified in each of the horizontal slices, are an approximation to so-called *normally hyperbolic invariant curves* [12]. Very little is known about the impact that such structures and associated manifolds have on 3D Lagrangian transport. See, however, [13] for a start on this important problem.

Answers to such basic questions as to the vertical extent of these special curves and whether inflow or outflow at one level of an ocean eddy is compensated or reinforced by flow at other levels are unknown. These questions are directly addressed for the first time here.

This report is organized as follows. The next section reviews Eckart's analysis discussed in [1]. Section 3 provides a brief tutorial that relates concepts from dynamical systems theory to continuum mechanics and to Eckart's analysis. This section is aimed at those who are interested in chaotic advection processes in fluids, but who may not be conversant with recent developments in geophysical fluid dynamics. In section 4 we apply the concepts outlined in §3 to data from a large anticyclonic eddy in the Gulf of Mexico. We identify *lobes* at the edge of the eddy that remain coherent deep into the water column and are responsible for the exchange of fluid between the eddy and its surroundings. The lobes are closed material regions delineated by intersecting segments of stable and unstable manifolds of hyperbolic trajectories (cf. §3). Their role in mediating transport via the so-called turnstile mechanism has been long recognized in dynamical systems theory (e.g., [14, 15, 16, 17, 18, 19, 20]). Applications of these ideas to fluid flows, mostly to relatively simple 2D time-dependent kinematic or numerical models, date back to the beginning of studies of chaotic advection ([21, 22, 23, 24, 25, 26, 5]). Applications to realistic ocean data, as considered here, are rare and the few published examples (see [27, 28, 11, 29])) were restricted to individual levels near the surface. Our analysis documents for the first time that lobes may exist from the surface down to at least 200m, the bottom of the eddy. Ramifications of this finding are discussed in the last section.

2. Eckart's Model for Stirring

The starting point of Eckart's [1] analysis is the classic advection-diffusion equation for a scalar C which can be written in Cartesian coordinates as

$$\frac{\partial C}{\partial t} + v_j \frac{\partial C}{\partial x_j} = \kappa \frac{\partial^2 C}{\partial x_j \partial x_j}. \tag{1}$$

As usual, the v_j are the three components of the fluid velocity while κ is the molecular diffusivity (assumed constant). The evolution of the gradient of the concentration, $G_i = \partial C/\partial x_i$, is governed by

$$\frac{\partial}{\partial t} G_i + v_j \frac{\partial G_i}{\partial x_j} + \frac{\partial v_j}{\partial x_i} G_j = \kappa \frac{\partial^2}{\partial x_j \partial x_j} G_i \,. \tag{2}$$

Finally, multiplying (2) by G_i and collecting like terms leads to

$$\left(\frac{\partial}{\partial t} + v_j \frac{\partial}{\partial x_j} - \kappa \frac{\partial^2}{\partial x_j \partial x_j} \right) G^2 + \left(\frac{\partial v_j}{\partial x_i} \right) G_i G_j = -\kappa \frac{\partial G_i}{\partial x_j} \frac{\partial G_i}{\partial x_j} \,, \tag{3}$$

where $G^2 = G_i G_i/2$. It will be useful later to express (3) as

$$\frac{\mathrm{d}}{\mathrm{d}t} G^2 + \left(\frac{\partial v_j}{\partial x_i}\right) G_i G_j = \kappa \left(\frac{\partial^2 G^2}{\partial x_i^2} - \frac{\partial G_i}{\partial x_j}\frac{\partial G_i}{\partial x_j}\right), \tag{4}$$

where $\mathrm{d}/\mathrm{d}t \equiv \partial/\partial t + v_i\,\partial/\partial x_i$ is the material derivative. Eckart [1] dealt mostly with the volume average of (3) or (4); however the analysis presented here will be local, so this step is irrelevant. Either way, (3) or (4), or their averages, provide considerable insight into the concept of Eckart's 'three regimes'.

The initial stage, according to Eckart, is characterized by an approximate balance between the local rate of change and advection of G^2, i.e. the dominant balance between the first two terms on the LHS of (3) or the first term of (4), with the remaining terms negligible. In this model the large scale and vortical motions gently distort the initial tracer distribution. The term, $(\partial v_j/\partial x_i)\, G_i G_j$, comes into play during the second phase of Eckart's analysis. Following Eckart, this stage is referred to as "stirring" in analogy to the stirring of cream in a cup of coffee. Eckart noted that since $(\partial v_j/\partial x_i)\, G_i G_j = 2 d_{ij} G_i G_j$, where d_{ij} is the symmetric deformation rate tensor, the vorticity plays a secondary role in this stage even if the flow is dominated by eddying motions.

Below we argue that the dynamics associated with this term is largely responsible for the intricate swirls and squirts commonly seen in coffee cups and satellite images of clouds and thermal patterns on the ocean surface. We emphasize this applies to the stirring phase in flows where $\kappa \lesssim \nu$ (ν fluid viscosity). This implies that the time scale for the large-scale advective transport is much less than the time needed to reach the diffusive limit from the initial large-scale tracer distribution. In this regime the tracer is spread over much of the flow domain yet it remains unmixed at small scales as discussed in [30]. The final stage in the Eckart's scenario is dominated by the two molecular diffusivity terms (i.e. those proportional to κ) in (3) or (4). The strong concentration gradients along highly convoluted fronts enhance molecular diffusion, and so in the final stage they produce a pleasant homogeneous mixture of coffee and cream.

Of course in fully turbulent 3D flows where velocity gradients increase with decreasing scale, the largest contribution to stretching is at small scales (e.g. [30]). Consequently, the time scale for molecular mixing within a 3D turbulent region is the same order of magnitude as the time scale for transport

across that region. In this case the evolution of a patch of tracer is dominated by small scale mixing and Eckart's 'second phase' is not well pronounced.

An interesting observation regarding the role of concentration gradients in Eckart's final stage can be made by transforming the advection-diffusion equation (1) into a tracer-based coordinate system so that one of the coordinates enumerates level sets of the tracer concentration (e.g. [31]). Such a transformation incorporates the reversible effects of pure advection within the coordinate system itself and leads to a pure-diffusion equation with an 'effective diffusivity', which quantifies the irreversible processes of advection and diffusion acting together on sufficiently small scales. The effective diffusivity coefficient is a function of G^2 and is usually minimal in the neighbourhood of Lagrangian transport barriers. We will return to this point at the end of §3.4.

3. Stirring and Dynamical Systems Theory

3.1. Background

Eckart's analysis is an Eulerian description of tracer dynamics in an underlying flow field. It is based on the advection-diffusion equation governing the evolution of the tracer concentration field. Applications based on numerical solutions of the governing equations generally rely on parameterizations of a diffusion coefficient tensor to account for unresolved, small scale advective processes. However, it seems more natural to think of the phenomenology of eddies, filaments, and the associated mass transport from a material or Lagrangian perspective. The framework for the Lagrangian description of fluid flows and tracer dynamics stems from dynamical systems theory.

In this regard one can start by formulating the Navier-Stokes equations as an infinite-dimensional dynamical system and analyze its properties in an abstract space spanned by coefficients of an appropriate functional expansion. In Lagrangian transport considerations, however, the emphasis is on a low dimensional velocity field in a physical space, which already satisfies the Navier-Stokes equations. In this framework one can consider the so called *fluid particle trajectories* which satisfy a two or three-dimensional non-autonomous dynamical system induced by the velocity field. Tracer trajectories coincide with the fluid particle trajectories only when the tracer diffusivity is identically zero. Otherwise, the advection-diffusion equation cannot be formally reduced to a hyperbolic equation whose characteristics are the fluid particle trajectories. The fundamental differences between these

approaches were first thoroughly studied by Truesdell ([32]). An assessment of the two approaches and the crucial role of initial conditions is overdue, but outside the scope of this study.

Stirring of a tracer, with which we are concerned here, refers to a process of advective redistribution of a nondiffusive tracer by an underlying velocity field. An important diagnostic in this approach is the separation of neighboring trajectories in phase space as quantified by Lyapunov exponents, LE. For an n-dimensional autonomous dynamical system a trajectory has n Lyapunov exponents. The one associated with a direction tangent to the trajectory is always zero with $n-1$ Lyapunov exponents are associated with the remaining directions. The LE measure the growth of infinitesimal perturbations in these directions, i.e. growth rates of the linearized dynamics about the trajectory (see [33, 34, 35] for more details). Of particular interest is the maximum LE since the existence of a single positive LE indicates that the trajectory is unstable. By this we mean that infinitesimal uncertainties in the initial conditions of a trajectory, including numeric truncation, will grow exponentially and ultimately dominate the solution if there is a positive LE.

Of course, the assumption of zero diffusivity which is inherent in the concept of stirring is unrealistic in most real-life applications. However, there exist a range of situations where stirring represents a good approximation of dominant transport processes, at least at certain stages of evolution and at appropriate spatial scales. Eckart's coffe cup example, as well as many laminar and quasi-turbulent geophysical flows fall into this category (e.g. [5]).

3.2. Stirring and Lagrangian structures in finite-time flows

Despite compelling similarities between stirring cream in a coffee cup and mesoscale tracer structures observed in oceanic flows, the application of the 'coffee cup paradigm' to geophysical fluid dynamics faces two conceptual obstacles. The obvious difference is that, in contrast to the ocean and atmosphere, the coffee cup dynamics is not influenced by the Coriolis force. The more subtle and fundamental issue is that the original concept of LE is based on infinite-time flow asymptotics. This, of course, is impossible to achieve in the Eckart-type geophysical fluid problem. Instead, a number of finite measures of trajectory separation are used. They all employ a Lyapunov-type formulation but are restricted to finite time intervals and, consequently, are easy to compute for any given flow.

Finite-time Lyapunov exponents ($FTLE$) are obtained by computing the rate of separation of trajectories with perturbed initial conditions, but the computation is restricted to a finite time interval. Of course, such a separation measure is sensitive to the length of the time interval over which the $FTLE$'s are calculated. Nevertheless, with appropriate caution the FTLE's often provide a useful diagnostics.

There are two classes of $FTLE$ fields for 2D flows. Forward FTLE fields are obtained at each time instant t_n within a time interval I by computing the $FTLE$'s for trajectories starting at every model grid point in forward time over time interval of length T. The grid points are then color coded according the the magnitude of the largest $FTLE$. Backward $FTLE$ fields are computed by reversing the direction of time. Note here that for any $t_n \in I$ it is possible to compute an $FTLE$ field for any T such that $t_n+T \in I$. Clearly this produces a non-unique $FTLE$ field at any t_n. Branicki and Wiggins [36] provide an extensive discussion of these issues.

It is not obvious what T should be used in applications, especially since the resulting $FTLE$ can vary significantly even for modest variations of T. Despite these limitations, ridges in forward $FTLE$ fields (i.e. maximizing curves of the scalar field) often indicate regions characterized by strong stretching in the direction normal to the ridge, and contraction along the tangent to the ridge [1]. Conversely, ridges in the backward $FTLE$ fields are usually hallmarks of Lagrangian flow structures characterized by contraction in the direction normal to the ridge, and stretching along the tangent to the ridge. The ridges in the forward $FTLE$ maps are referred to as repelling *Lagrangian Coherent Structures* (LCS) [38, 37] and ridges in the backward $FTLE$ maps are referred to as attracting LCS.

The LCS describe regions of very high stretching/contraction. Consequently, they are not general flow-invariant (hereafter material) manifolds, although they may be useful surrogates in certain regions of the flow as noted by [39]. Moreover, [36] show that $FTLE$ ridges are leaky, particularly in flows undergoing rapid transitions, and that their utility is often sensitive to the time interval over which they are calculated. Nevertheless, segments near

[1] As noted in [37] lines of high shear also produce strong ridges in the $FTLE$ fields. However, such high shear structures are not associated with the stretching/contraction dichotomy.

intersections of strong ridges of forward and backward $FTLE$ fields usually closely approximate material manifolds. We exploit this property in §4.

Dynamical systems theory provides a paradigm for identifying certain distinguished trajectories that are important in diagnosing Lagrangian transport. A characteristic of these special trajectories is that they must lie on an intersection of two material manifolds. One manifold contains particles moving away from the distinguished trajectory, initially at an exponential rate, while the other manifold contains approaching particles. In contrast to the ridges of the $FTLE$ fields, such manifolds are a priori barriers to transport since they are computed as curves composed of fluid particles.

In steady, two-dimensional flows these manifolds are easy to identify. Suppose, for example, the velocity field in a neighborhood of a stagnation point (i.e. a point $\boldsymbol{x}_0$ such that $\boldsymbol{v}(\boldsymbol{x}_0) = 0$) is given by $v_1 = \lambda x$, $v_2 = -\lambda y$. Trajectories produced by this flow that start on the x, y axes remain confined to these axes. Those starting on the x axis are repelled exponentially from the origin just as those that start on the y axis are attracted exponentially towards the origin. In dynamical systems terminology the x and y axes are examples of, respectively, *unstable* and *stable* manifolds of the saddle-point $(x, y) = (0, 0)$ that separate particles by their fates. Particles in the right and left half-planes are repelled from the ordinate while those in the upper and lower half planes are attracted towards the abscissa; no trajectory can cross the x and y axes.

Explicit time dependence in the flow provides a bit of complication. Ide et al [40] and Kirwan [41] give a number of simple examples illustrating this problem. In the time-dependent setting the paths of instantaneous stagnation points (ISPs) given by curves $\boldsymbol{x}_{isp}(t)$ such that $\boldsymbol{v}(\boldsymbol{x}_{isp}(t), t) = 0$, do not necessarily correspond to particle trajectories. As a consequence, paths of ISPs are not material objects and they cannot be used in Lagrangian transport considerations. The 'true' analogues of the saddle stagnation points in time-dependent flows are hyperbolic trajectories (see [42, 40]). This analogy is due to the fact that hyperbolic trajectories, just as saddle stagnation points, lie on intersections of stable and unstable manifolds. However, the geometry of the manifolds associated with hyperbolic trajectories is time-dependent. For example, in 2D time-dependent flows the instantaneous geometry of stable and unstable manifolds is given by two material curves that intersect at a moving hyperbolic trajectory. Moreover, in contrast to the steady 2D case, these manifolds can intersect along a multitude (possibly a countable infinity) of hyperbolic trajectories. See figure 1).

It turns out, however, that not all of these hyperbolic trajectories are equally important. The so-called Distinguished Hyperbolic Trajectories (DHTs) play a role of organizing centers in the flow and their stable and unstable manifolds form dominant tangles (i.e. the heteroclinic or homoclinic tangles) serving as a template for the Lagrangian transport. For slowly changing velocity fields Haller and Poje [43] showed that one can locate paths of ISPs in the neighborhood of distinguished hyperbolic trajectories. This is useful since stagnation points are easy to determine in flow fields, whereas there is no simple diagnostic for the location of the hyperbolic trajectory. However, it is noted that the linearization of the instantaneous velocity field in the neighborhood of a DHT generally does not yield a saddle-like flow structure (see [40] for examples).

Despite the existence of algorithms for computing DHTs in aperiodically time-dependent flows, see [40, 44], their utility to diagnose local scale processes is limited. The limitations arise mainly from difficulties in identifying the most important (or distinguished) hyperbolic trajectories. See [36] for more details. Consequently, there are a variety of ad hoc, and usually labor intensive, methods to identify the stable and unstable manifolds in time dependent flows. See [25] for additional discussion and references.

3.3. Lagrangian eddies and their lobes

In order to delineate eddies, squirts, and filaments, it is necessary to determine their appropriate boundaries. The key issue is what constitutes *appropriate*? Eulerian definitions of these structures usually are based on isocontours of appropriate scalar fields such as tracer concentration or temperature or sea surface height. Of course, these contours generally are not material objects and it is questionable to infer mass or heat transport based on their deformation. Identification of the desired material eddy boundary also poses a challenging task. After all, one may construct an universe of material manifolds in any flow by following an evolution of simple material segments. Note also that if an eddy boundary is given by a closed material loop, transport across such a boundary is impossible by definition. Although, such a choice of an eddy boundary might seem attractive at first, a material eddy boundary would quickly become greatly deformed and spread, rendering the notion of a localized eddy ambiguous. The construct used here represents an attempt to reconcile the requirement for a material boundary with a possibility of mass exchange between a localized eddy and its environment. It was first proposed by [29] but the general concept (related to the so-called

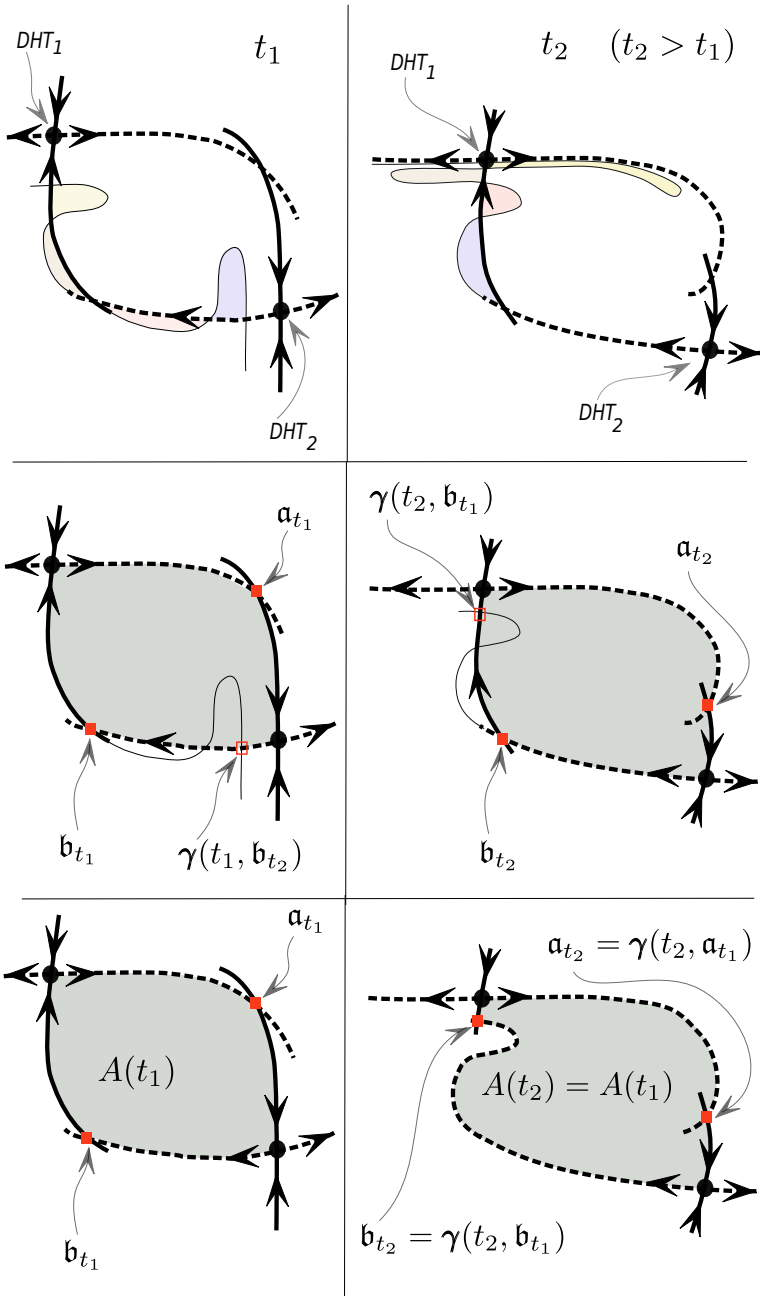

Figure 1: A sketch illustrating 2D instantaneous geometry, at two different times t_1 and t_2, of a time-dependent Lagrangian eddy and its turnstile lobes (top row; color-shaded) which mediate transport in and out of the eddy. The eddy is delineated by intersecting segments of time-dependent stable (solid) and unstable (dashed) manifolds of two Distinguished Hyperbolic Trajectories. Note that if the boundary intersection points (filled red squares) are chosen such that $\mathfrak{a}_{t_2} = \boldsymbol{\gamma}(t_2, \mathfrak{a}_{t_1})$, $\mathfrak{b}_{t_2} = \boldsymbol{\gamma}(t_2, \mathfrak{b}_{t_1})$ (bottom row), the eddy boundary remains a material contour throughout the evolution which inhibits any transport. ($\boldsymbol{\gamma}(t, \boldsymbol{x}_0)$ denotes a (fluid particle trajectory such that $\boldsymbol{\gamma}(t_0, \boldsymbol{x}_0)) = \boldsymbol{x}_0$.)

resonance zones) originates from the work on transport in 2D area-preserving maps (e.g. [15, 45]) and 3D volume-preserving flows [46, 47].

Here a Lagrangian eddy is defined as a closed region bounded by intersecting material (stable and unstable) manifolds emanating from two DHT's (see figure 1). Perhaps the least intuitive aspect of this construct is that the interior of a Lagrangian eddy is not coherently defined throughout its evolution, since the intersections between pairs of manifolds closing the boundary are not fixed, i.e. they are not flow-invariant as explained below. This property is, in fact, crucial in facilitating transport in and out of the eddy (see [42] for more details). Figure 1 is a cartoon of eddy geometry sketched at two different times. The instantaneous geometry of entangled stable and unstable manifolds of the two DHT's is represented by the black curves. Every point making up these manifolds at $t = t_1, t_2$ corresponds to a distinct trajectory at the respective time. Note that a point of intersection between any two material manifolds remains on an intersection throughout the evolution (i.e. every such an intersection is a trajectory). Thus, closed regions bounded by the intersecting segments of the manifolds in figure 1 form *material lobes* (color-coded areas in figure 1) whose evolution provides the main mechanism for mediating eddy-induced Lagrangian transport via the turnstile mechanism as described, for example, by [42]. The choice of the boundary intersection points (bips) determine the eddy interior (figure 1, two bottom rows). Since the respective manifolds intersect multiple times, this choice is clearly non-unique.

Here we chose the bips $\mathfrak{a}(t_{1,2})$ and $\mathfrak{b}(t_{1,2})$ so that a two-lobe turnstile (purple-magenta) 'flips' between the eddy interior and exterior at some time within the interval $[t_1, t_2]$. A similar procedure is used to visualize turnstile transport in §4. The exact identification of the eddy interior is largely irrelevant for our purposes[2] since the underlying topological constraints associated with the evolution of turnstile lobes in such a heteroclinic tangle imply that the turnstile flip must occur as it approaches a DHT along the respective stable manifold (see [16, 42]). Note finally that requiring the two bips to be *flow invariant* (i.e. fixed to two trajectories $\boldsymbol{\gamma}_\mathfrak{a}$ and $\boldsymbol{\gamma}_\mathfrak{b}$ so that $\mathfrak{a}(t) = \boldsymbol{\gamma}_\mathfrak{a}(t, \mathfrak{a}_{t_1})$, $\mathfrak{b}(t) = \boldsymbol{\gamma}_\mathfrak{b}(t, \mathfrak{b}_{t_1})$), as illustrated in the bottom row of figure 1, is equivalent to creating a material loop and prohibiting transport across such a boundary.

[2]We note that there exist coherent criteria for determination of bips; see for example [48, 42].

We readily acknowledge that a Lagrangian construct cannot always be associated with every eddy-like structure observed in the Eulerian frame. Nevertheless the notion of a material eddy boundary defined above can yield crucial insight into how eddy type flow structures can maintain some coherence while exchanging fluid with their environment.

A number of authors (e.g. [49, 50, 5]) have used the *lobe dynamics* approach to study basin scale transport in simple dynamic models. Detection of lobes in synoptic data sets and realistic ocean models has not been as successful. The only published examples we are aware of are [11] and [28] (see also [29] for more details).

3.4. Finite-time Lapunov Exponents and Eckart's analysis

What then is the connection of $FTLE$ framework to Eckart's analysis? Recall he established that the crucial diagnostic in the intermediate stage was based on the fluid deformation rate. On the other hand the separation of neighboring fluid parcels in a flow is characterized by the right Cauchy-Green deformation tensor, Δ. The properties of this tensor relevant here can be derived as follows: Given a fluid parcel trajectory $\boldsymbol{\gamma}(t, \boldsymbol{x}, t_0)$ passing through $\boldsymbol{x}$ and a small perturbation, $\boldsymbol{\delta}_{\boldsymbol{x},t_0}$, at time $t = t_0$, the separation distance at time $t = t_0 + T$ is given by (e.g. [39])

$$||\boldsymbol{\delta}_{\boldsymbol{x},t_0}(T)|| = \sqrt{\langle \boldsymbol{\delta}_{\boldsymbol{x},t_0}, \Delta_{T,t_0}(\boldsymbol{x})\, \boldsymbol{\delta}_{\boldsymbol{x},t_0} \rangle}, \tag{5}$$

where $\langle \cdot, \cdot \rangle$ denotes the canonical scalar product and $\boldsymbol{\delta}_{\boldsymbol{x},t_0}(t_0) \equiv \boldsymbol{\delta}_{\boldsymbol{x},t_0}$. The Cauchy-Green tensor can be expressed in terms of a *flow-induced map*, $\Phi_{t_0}^{t_0+T}$, as

$$\Delta_{T,t_0}(\boldsymbol{x}) = \left(\partial_{\boldsymbol{x}} \Phi_{t_0}^{t_0+T}(\boldsymbol{x})\right)^{\dagger} \partial_{\boldsymbol{x}} \Phi_{t_0}^{t_0+T}(\boldsymbol{x}), \tag{6}$$

where $\dagger$ denotes the matrix transpose, $\Phi_{t_0}^{t_0+T}(\boldsymbol{x}) = \boldsymbol{\gamma}(T, \boldsymbol{x}, t_0)$, and $\partial_{\boldsymbol{x}} \Phi_{t_0}^{t_0+T}(\boldsymbol{x})$ denotes the Jacobian of $\Phi_{t_0}^{t_0+T}$ evaluated at $\boldsymbol{x}$. Since Δ is symmetric and positive definite, its eigenvalues are real and its eigen-directions, corresponding to the maximum and the minimum stretching, are orthogonal. The largest forward and backward $FTLE$ for a fluid parcel trajectory $\boldsymbol{\gamma}(t, \boldsymbol{x}, t_0)$ are then expressed as

$$\mathfrak{f}_{t_0}^{t_0 \pm T}(\boldsymbol{x}) = \frac{\ln\left[\lambda^{(+\,-)}(t_0, \boldsymbol{x})\right]}{2\,T}, \tag{7}$$

where $\lambda^{(+\,-)}$ is the largest eigenvalue of the (time-forward/backward) Cauchy-Green tensor, indicating the direction of maximum stretch in a frame moving

with the trajectory $\boldsymbol{\gamma}$ in the extended phase space, spanned by the spatial directions and time. The largest LE is simply the limit of (7) as $T \to \infty$.

Recall now that the rate of change following the flow of the square of the separation distance, $||\boldsymbol{\delta}_{\boldsymbol{x},t_0}(t)||$, between two neighboring fluid parcel trajectories is given by

$$\frac{\mathrm{d}}{\mathrm{d}t}||\boldsymbol{\delta}_{\boldsymbol{x},t_0}(t)||^2 = \langle \boldsymbol{\delta}_{\boldsymbol{x},t_0}(t), \hat{D}(t,\boldsymbol{x})\, \boldsymbol{\delta}_{\boldsymbol{x},t_0}(t)\rangle, \tag{8}$$

where $\hat{D}$ is the deformation rate tensor (see, for example, [51, 38]) with components

$$d_{ij}(t,\boldsymbol{x}) = \frac{1}{2}\left(\frac{\partial v_i(t,\boldsymbol{s})}{\partial s_j} + \frac{\partial v_j(t,\boldsymbol{s})}{\partial s_i}\right)\Bigg|_{\boldsymbol{s}=\boldsymbol{\gamma}(t,\boldsymbol{x},t_0)}. \tag{9}$$

Equation (8) provides an alternative expression for the separation distance (cf. (5)) in the form

$$||\boldsymbol{\delta}_{\boldsymbol{x},t_0}(T)||^2 = \int_{t_0}^{t_0+T} \langle \boldsymbol{\delta}_{\boldsymbol{x},t_0}(\tau), \hat{D}(\tau,\boldsymbol{x})\boldsymbol{\delta}_{\boldsymbol{x},t_0}(\tau)\rangle \mathrm{d}\tau + ||\boldsymbol{\delta}_0||^2. \tag{10}$$

Consider now the evolution of the passive tracer during the second stage in Eckart's analysis. As discussed in §2, this is characterized by an approximate balance between the first two terms in (4). Thus, upon neglecting the diffusive terms in (4), and noting that $(\partial v_i/\partial x_j)G_iG_j = 2d_{ij}G_iG_j$, the approximate balance can be written as

$$\frac{\mathrm{d}\boldsymbol{G}^2}{\mathrm{d}t} = -2\langle \boldsymbol{G}, \hat{D}\,\boldsymbol{G}\rangle. \tag{11}$$

Clearly, the forward-time evolution of (8) is the same as the backward-time evolution of (11). We stress here that the similarity between (8) and (11) holds only during the second phase of the three-regime partition of flow evolution discussed in §2. This analogy breaks down when molecular diffusion rivals the advective transport.

What are the implications on the tracer dynamics in the neighborhood of a ridge in the backward FTLE field? Recall that such ridges usually indicate strong separation over a time interval $-T$ of fluid parcel trajectories in the direction normal to the ridge and a convergence along the tangent to the ridge. Equations (8) and (11) indicate that concentration gradients tend to

be quickly amplified in forward time along the normals to the ridges of $\mathfrak{f}_{t_0}^{t_0-T}$. In this configuration the stretching (and folding) occurs along the $FTLE$ ridges, which are aligned with closely spaced isolines of tracer concentration.

It is important to note here that since the $FTLE$ ridges are based on finite-time diagnostics, the degree of such an alignment is affected by transitions in the flow and the time window chosen for the $FTLE$ computations. Nevertheless, this geometry greatly increases the contact area between the tracer and ambient fluid, thus ultimately promoting molecular diffusion. The similarity of this scenario with the transition between the second and third phases of Eckart's paradigm is noteworthy.

3.5. Lagrangian structures in three-dimensional finite-time flows

What about three-dimensional flows? Recently, techniques were developed to identify stable and unstable manifolds of hyperbolic trajectories [52] and the ridges of the FTLE fields [53] in 3D time-dependent flows. However, the Lagrangian transport analysis via the lobe dynamics in 3D aperiodically time-dependent flows is currently at a nascent stage of development. Moreover, as operational forecasting models of ocean circulation currently do not calculate vertical velocities as a primitive variable, the use of these techniques is limited.

Here we choose an approach that is based on quasi-2D analysis in horizontal layers that are vertically stacked in the 3D velocity field. Obviously this approach is fully justified when the vertical velocity is zero. Even if this is not strictly true, there are two distinct cases where the quasi-2D analysis in stratified oceanic flows is justified. It was shown in [29] that the 2D Lagrangian analysis of a 3D flow can be extended to a layer whose thickness H is chosen such that the ratio, say ϵ, between an average vertical shear of the horizontal velocity components to the average horizontal velocities within the layer is small (i.e. $H\epsilon \ll 1$). If such a configuration is identified, one can construct approximate transport barriers by vertically extending the invariant manifolds computed in the 2D slice to the whole layer. While the tracer trajectories can move in the vertical within such material surfaces (or even leave the layer), the overall 'wall-like' geometry remains coherent, allowing for approximate transport analysis within the layer.

There also are theoretical arguments that support another type of quasi-2D analysis, which can be justified when vertical velocities are small relative to the horizontal velocity scales. Mezic & Wiggins [13] discuss the consequences of perturbing a stratified horizontal velocity field with a weak vertical

component. They show that in such cases the curves traced by instantaneous locations of hyperbolic trajectories identified in each of the horizontal layers can persist in the perturbed flow and give rise to *normally hyperbolic invariant curves* (NHC). In 3D, time-dependent, incompressible flows the NHC have stable and unstable manifolds that, at any fixed time, are given by two surfaces intersecting at the NHC. The analysis in a fixed horizontal layer therefore provides information on the geometry of the cross-section of such manifolds with the given layer. Can such hyperbolic curves exist in geophysical scale flows such as the Gulf of Mexico? Do they play a role in shaping the 3D structure of the large vortex rings commonly observed in such flows? These questions are explored in the analysis below.

4. Application to Juggernaut

We now illustrate how Lagrangian techniques can aid in the analysis of advective transport in realistic ocean data with an example drawn from the Gulf of Mexico. The circulation of the near surface in the Gulf is known to be dominated by large anticyclonic (counterclockwise rotating) eddies or rings, [54]. These rings are among the largest eddies in the world ocean. Diameters of the order of 300 km (based on the Eulerian metrics) and swirl velocities greater than two meters per second have been reported, [55, 56]. The rings are pinched off from the Loop Current, a part of the North Atlantic western boundary current system, at irregular intervals and migrate westward.

The ultimate fate of these rings is a subject of an ongoing dispute. Non-data assimilating circulation models [57], [58], [59] show rings migrating clear across the Gulf and slowly decaying along the western continental slope (commonly referred to in this context as the 'eddy graveyard'). Typical ring lifetimes in these models are of the order of one year. However, Kantha [59] noted that when these models are run with data assimilation, the surface signature of these rings is lost in midgulf. Typical lifetimes are of the order of a few months. Lipphardt et al [60] studied three of the 12 named rings in [59] using a variety of dynamical-systems-based Lagrangian methods. They linked the abrupt disappearance of the ring signatures at 50m to the emergence of stable and unstable manifolds emanating from nearby hyperbolic regions. Although these regions were not explicitly analyzed for such structures, they most likely contained distinguished hyperbolic trajectories. Curiously, the filaments developed from this process strongly resembled that of cream in coffee during Eckart's stirring phase.

Our analysis uses hindcasts made from the Colorado University Princeton Ocean Model, CUPOM, the same data source used by [60] and earlier by [61] in a study of the predictability of the ocean. This model is a three-dimensional, primitive equation, 24 sigma level curvilinear grid version of the Princeton Ocean Model [62], [63] with a mixed layer two equation second moment closure of turbulent mixing [64], [65]. The model incorporates free surface dynamics through a split mode technique, and a horizontal diffusion that follows the Smagorinsky [66] scheme. The horizontal grid is a staggered Arakawa C grid with one-twelfth degree resolution. The vertical grid is terrain following with bottom topography specified from ETOP05. The model calculates the 2D velocity in the sigma layers along with the temperature and salinity fields. These coordinates are commonly used in general circulation models because they follow the ocean bottom terrain, consequently simplifying bottom boundary conditions. Thus they are preferable to potential density or spherical coordinates, which intersect sloping bottoms. However, to conform with data on ocean eddies we transform model output into a latitude, longitude, z system. Moreover, the differences between z and ρ coordinates tend to be small in the ocean interior.

As with most data assimilating forecast models the vertical velocity, i.e. the velocity normal to the sigma surfaces, is not a primary variable in CUPOM. This field can be inferred from the continuity equation, however that calculation introduces additional numerical errors. Moreover, vertical velocities inferred from the continuity equation are typically several orders of magnitude smaller than the horizontal velocities. We have calculated these fields in other applications and found them quite 'noisy' and unreliable for the analysis used here.

CUPOM is well validated with independent Eulerian data, see [65]. Unlike many data assimilating models it has also been tested against independent Lagrangian [67] and ocean color [68] data in the eastern Gulf. Because CUPOM is exercised with full data assimilation and has been so well validated in this region, we regard it as an interpolation engine that produces dynamically consistent maps of ocean currents from observations.

The size and relatively large velocities associated with the Loop Current Rings pose threats to offshore oil operations. Consequently the Minerals Management Service and the offshore oil industry formed the Climate and Simulation of Eddies and the Eddy Joint Industry Project (CASE/EJIP) consortium that monitors the formation and migration of the Loop Current Rings in the Gulf of Mexico. This consortium assigns names to individual

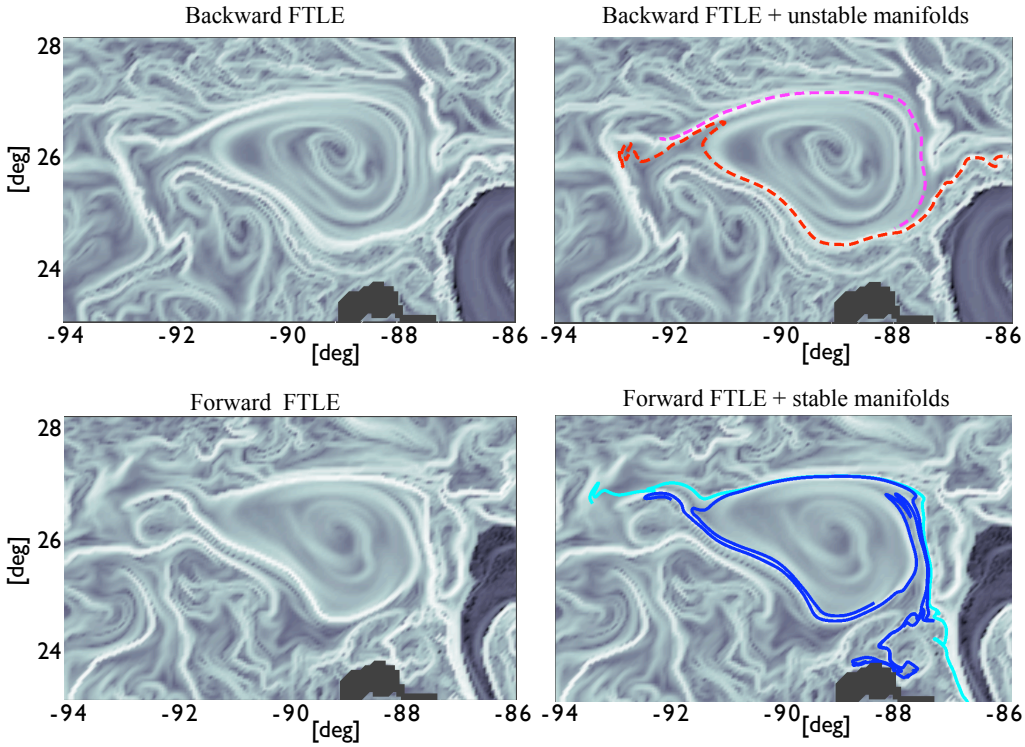

Figure 2: Comparison of the FTLE fields (cf. §3.2) on 3 December 1999 ($T = 12$ days) and the instantaneous geometry of unstable manifolds (top row) and stable manifolds of the two DHTs associated with the Juggernaut eddy. The intersections (not shown) of strong ridges in the forward and the backward FTLE maps help to identify the two DHTs. The computed manifolds overlap with the FTLE ridges sufficiently close to the DHTs but thread together several strong FTLE ridges at larger distances from the DHTs. The strong current regime in the southeast corner of the figure is the Loop Current.

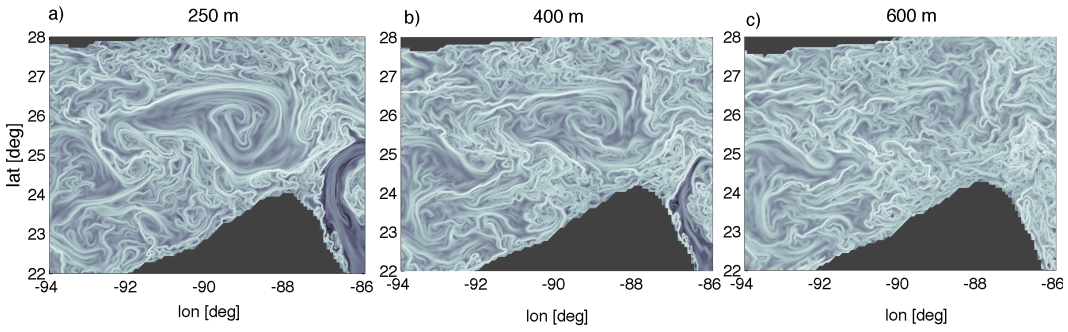

Figure 3: Backward FTLE fields computed in the Gulf of Mexico on December 3rd, 1999 at three different depths: 250m, 400m and 600m (integration time used in the computations $T = 10$ days. Note that the ridge structure characteristic of the eddy disappears at 600m. At depths greater than 250m, computations of intersecting stable and unstable manifolds, delineating the Lagrangian eddy, were inconclusive.

rings. The focus here is on Juggernaut. According to Kantha et al. [59] this ring was pinched off from the Loop Current on 8 October 1999. There is, however, some uncertainty in its disappearance. Using CUPOM, Kantha et al. [59] tracked the Juggernaut until 11 April 2000. But, using Lagrangian analysis, Lipphardt et al. [60] were only able to track it till 6 March 2000. The fate of this ring is not material to our analysis, which focuses on the period 3 -13 December 1999. During this period Juggernaut was about 100 km west of Florida.

To gain insight into the Lagrangian structure of Juggernaut during this period, we first calculated the $FTLE$ (see §3) at eight depths between 50 and 200 meters from the CUPOM velocity field for the region in the eastern Gulf of Mexico in the vicinity of Juggernaut. The forward and backward $FTLE$s showed robust intersections on the eastern and western tips of Juggernaut at all levels until about 250 meters. Using these intersections as the initial guesses for the locations of DHTs in each level, we then calculated stable and unstable manifolds in the horizontal slices down to 200 meters, using methods developed in [40, 69], and [44]. While the $FTLE$ fields were quite helpful in identifying the locations of the DHTs, the ridges of these fields did not provide sufficiently detailed information about the Lagrangian eddy geometry to assess transport.

Figure 2 shows a comparison of the backward and forward $FTLE$ fields on 12 December 1999 and the instantaneous geometry of unstable manifolds (top row) and stable manifolds of the two DHTs associated with Juggernaut. The computed manifolds thread together several strong ridges in the respective $FTLE$ fields. Increasing the integration time interval T produced more pronounced ridges but it also changed their location and connectivity (cf. §3.2 and [36]). Regardless of the chosen T, the $FTLE$ fields did not show the detail seen in the manifold computations. However, as suggested earlier, this technique proved to be useful in identifying Lagrangian signatures of Juggernaut.

Figure 3, shows three backward $FTLE$ fields computed at depths greater than those where a closed eddy area could be delineated by the stable and unstable manifolds of respective DHTs. Although the eddy silhouette is still visible between 250 and 400 meters, it rapidly fades at greater depths. We were unable to identify DHTs whose manifolds delineated a closed eddy at depths greater than 250 meters. Identification of robust intersections of the backward and forward ridges of the $FTLE$ fields, also became ambiguous at these depths.

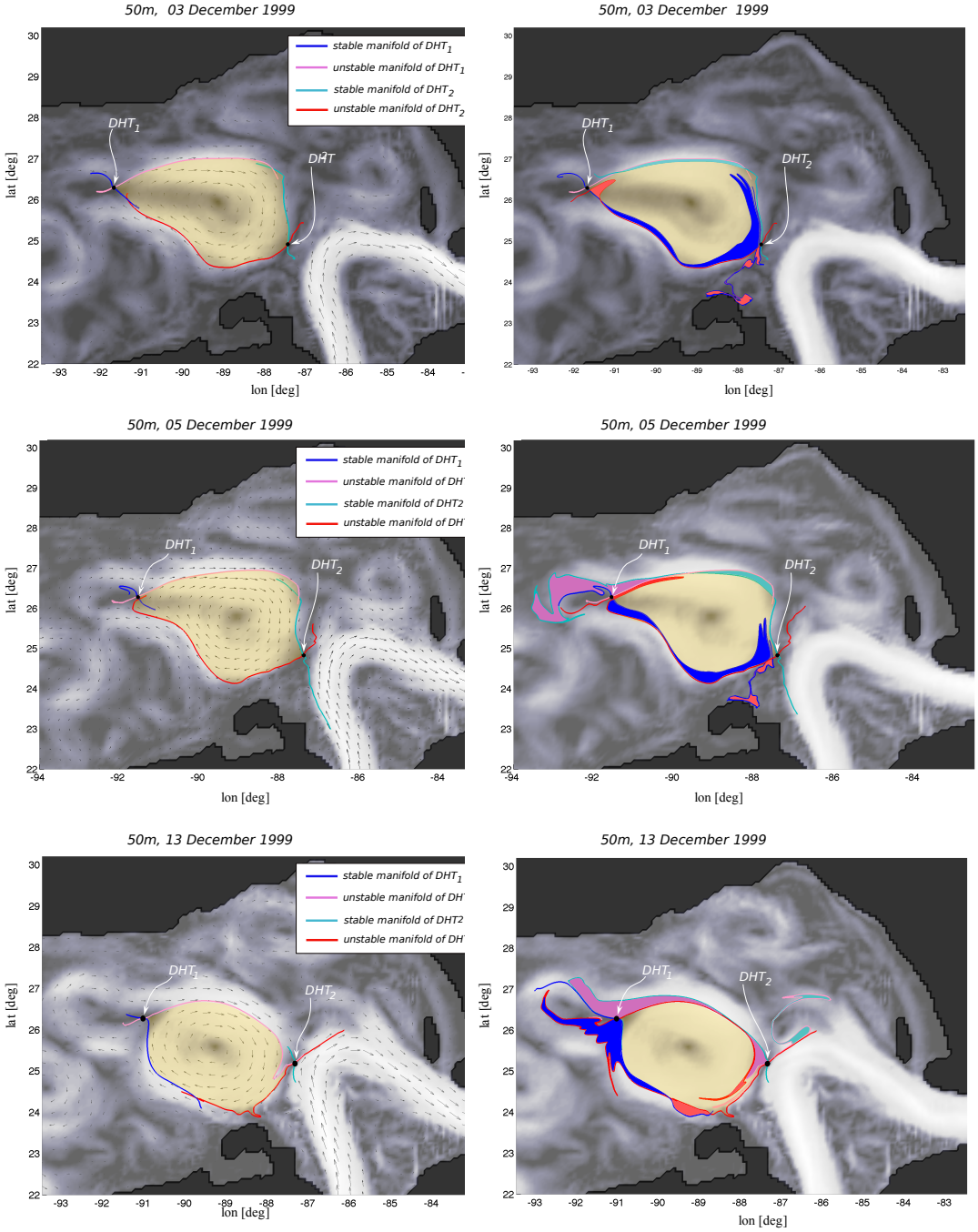

Figure 4: A sequence of snapshots showing the instantaneous geometry at 50m of stable and unstable manifolds of the two DHTs used to delineate the Lagrangian geometry of Juggernaut. The left column shows the eddy bounded by segments of the stable and unstable manifolds at three different times. The right column shows the corresponding lobe structure. The grayscale background indicates a relative magnitude of the instantaneous velocity field. A 3D instantaneous geometry of this eddy is shown in figure 7.

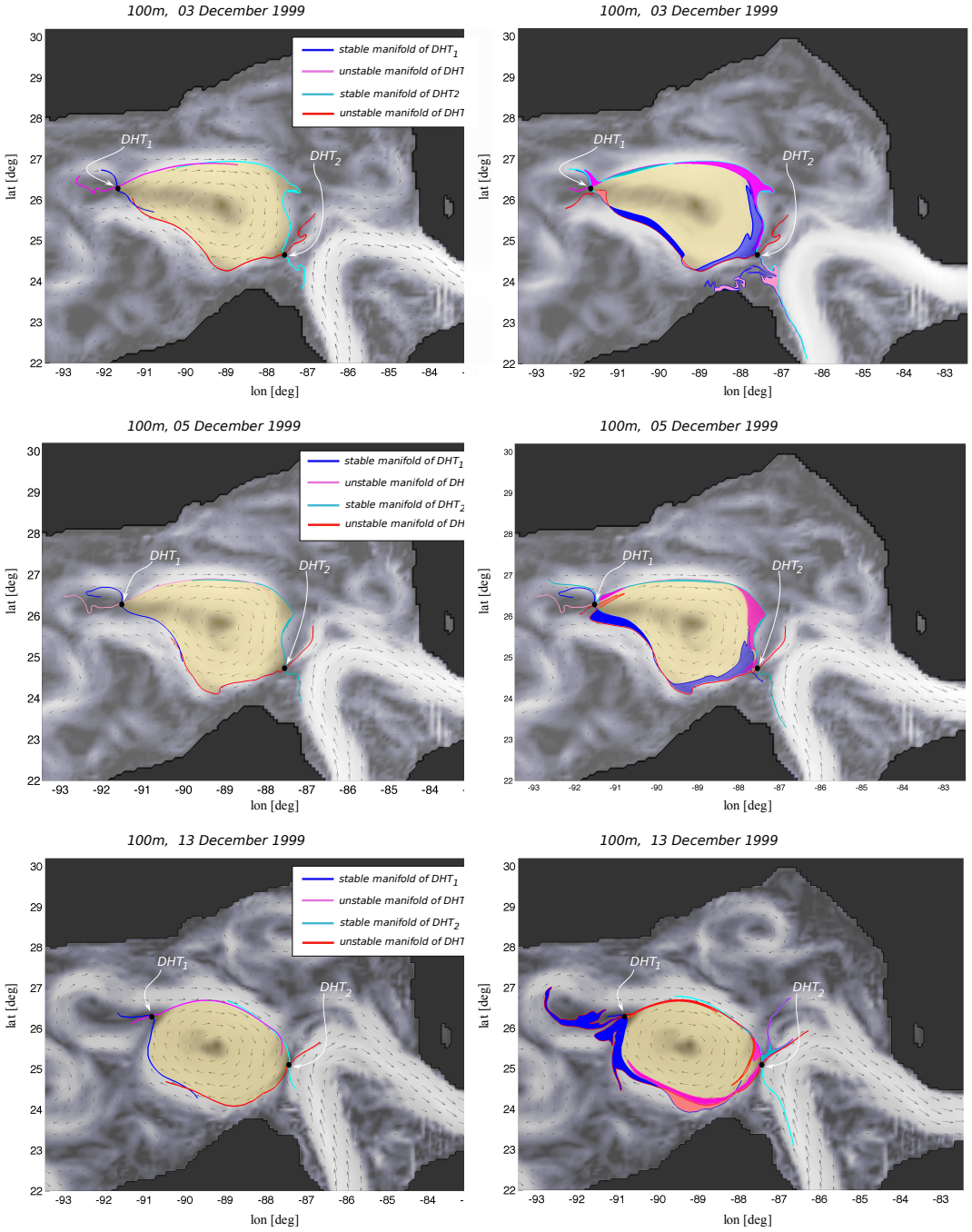

Figure 5: A sequence of snapshots showing the instantaneous geometry at 100m of stable and unstable manifolds of the two DHTs used to delineate the Lagrangian geometry of Juggernaut. See figure 7 for a 3D snapshot of this eddy.

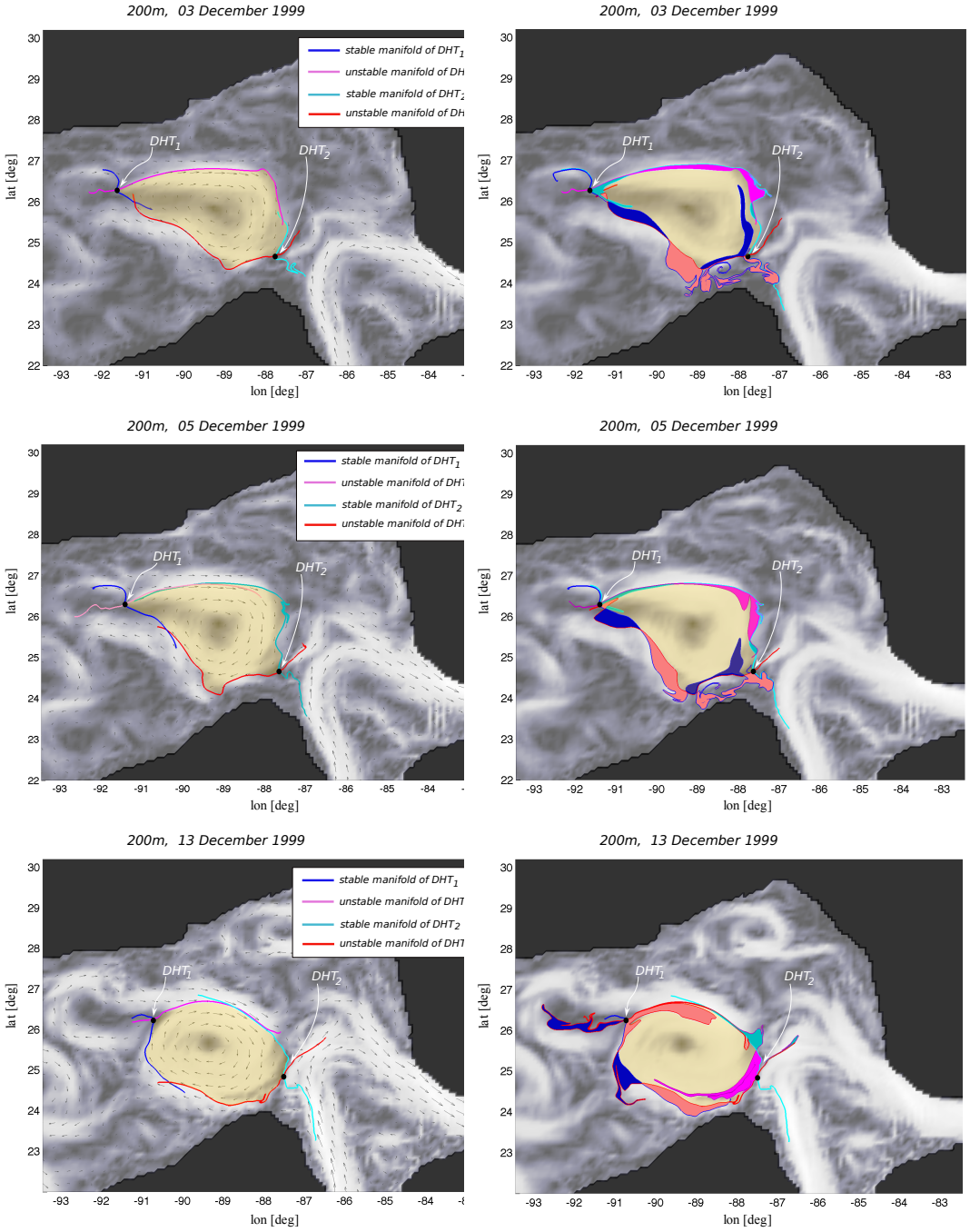

Figure 6: A sequence of snapshots showing the instantaneous geometry at 200m of stable and unstable manifolds of the two DHTs used to delineate the Lagrangian geometry of Juggernaut. See figure 7 for a 3D snapshot of this eddy.

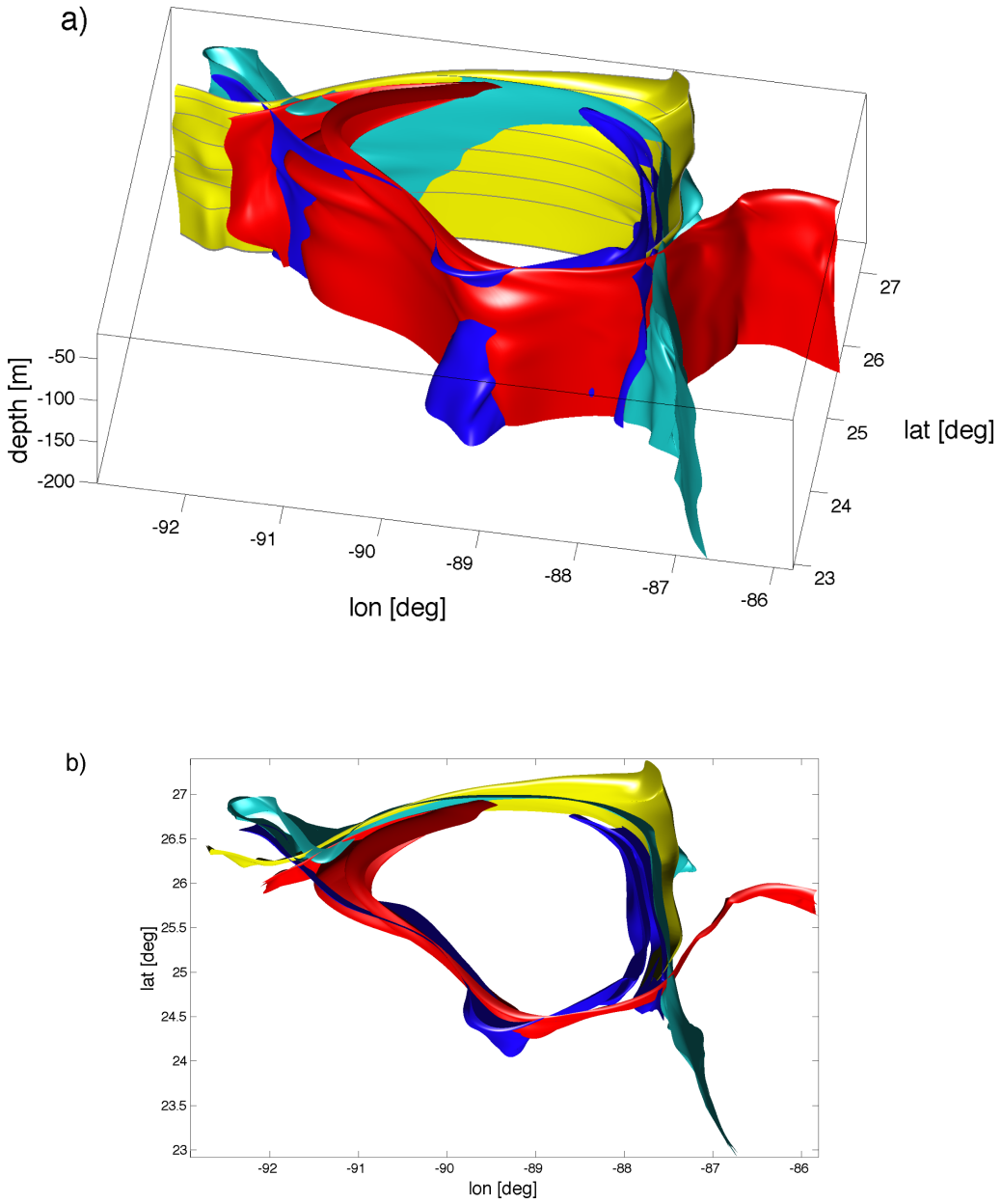

Figure 7: 3D instantaneous Lagrangian geometry of Juggernaut on 3 December, 1999; (a) side view, (b) top view. This geometry was obtained by computing the 2D manifold structure at eight depths: 20m, 30m, 50m, 75m, 100m, 125m, 150m and 200m and cubic interpolation in the vertical (the computational slices are marked on the yellow manifold). This eddy extends in the water column down to over 200m and stirs surrounding waters via the turnstile mechanism shown in figures 4-6.

Figure 4 shows a sequence of snapshots (on 3, 5, and 13 December 1999) of the instantaneous geometry of the stable and unstable manifolds associated with the two distinguished hyperbolic trajectories, DHT_1 and DHT_2, at 50m (the two black dots on the eastern and western edges). The left column shows the manifolds bounding the eddy. The right column in this figure shows the corresponding lobes. The lobes, which are suggestive of the finger-like structures in Eckart's analysis, are color coded according to the manifold segment which bounds them in the eddy's interior. Note that the evolving lobes are confined at the boundary region of the ring. This is also the region of the ring front, i.e. the strongest gradients in the density field, which are directed away from the center of the ring. This geometry is consistent with the configuration described in section 3 for the maximum distortion of the concentration field. The sequence shown in this figure shows how fluid is transported in and out of the eddy vie the turnstile mechanism near the two DHTs.

The northern lobe (magenta), formed by the intersection of the unstable manifold of DHT_1 and the stable manifold of DHT_2 is seen to transport fluid into the ring during the period 3 - 13 December 1999. Similarly the southern lobe (blue), formed from the intersections of the stable and unstable manifolds of DHT_1 and DHT_2 respectively eject fluid from the ring to the environment to the west. The highlighted segments of the stable and unstable manifolds of these two DHTs completely envelope the ring during this period, thus providing a Lagrangian characterization of its boundary.

Figures 5 and 6 show the same situation at 100m and 200m respectively. Note that the locations of the DHT_1 and DHT_2 at these levels are nearly the same as at 50m and the manifolds also completely enclose the ring. We note that within the three levels shown in figures 4-6 the area of the lobe intersections which are entrained into the eddy increases with depth and the area of the lobe intersections detrained from the eddy decreases with depth. This suggests that there is net fluid entrainment near the base and net detrainment in the upper portion of Juggernaut. The methodology described here offers a way to assess the vertical extent of the entrainment/detrainment in Juggernaut. We hope to report on this in subsequent papers.

Finally, in figure 7 we show the instantaneous 3D geometry of Juggernaut reconstructed from the manifold computations at eight different levels: 20m, 30m, 50m, 75m, 100m, 125m, 150m and 200m. Unlike some lens shaped eddy models it is noted that Juggernaut is only slightly bowl shaped as the area enclosed by the manifolds at 20m is only slightly larger than that at 200m.

This figure shows two striking features of Juggernaut. The first is the instantaneous 3D structure of the lobes formed from the intersection of the stable and unstable manifolds emanating from DHT_1 and DHT_2 at different depths. The instantaneous geometry of these manifolds is given by 2D surfaces that extend nearly vertically into the water column to the base of the eddy. The lobes formed by these manifolds and seen as elongated volumes were shown in the 2D slices presented in figures 4-6 to entrain fluid into the eddy along the northern edge and expel fluid along the southern edge.

The other striking feature is the intersection of the stable and unstable manifolds along the nearly vertical attracting/repelling "strings" which extend down into the water column. Recall that in 2D time-dependent fluid flows hyperbolic trajectories and their stable and unstable manifolds are represented, respectively, by curves and surfaces in the extended phase space formed by combining the two spatial dimensions and time. In this representation the two surfaces intersect along a curve which is exactly the hyperbolic trajectory. However, the situation analysed here corresponds to a 3D stratified flow and the manifold structure shown in figure 7 reveals the instantaneous geometry of the eddy. Consequently, the manifold intersections shown there are not trajectories. In fact, these structures are really an approximation of a NHC, as discussed in §3.5. We find it remarkable that these curves and the associated manifolds are approximately vertical.

There are two potentially important implications of this calculation. The first is the need to quantify the net fluid exchange between eddies and their environments. This will determine the importance of this mechanism on eddy dynamics and in transport of heat and salinity in the world ocean. If the turnstile mechanism is important then present views of geophysical turbulence will require considerable modification. Achieving this goal will require substantial additional analyses and routines. We hope to report on this in later studies. Second, it raises the question as to what are the dynamics responsible for this phenomena. Earlier it was observed that the manifolds are located along at the edge of the eddy, which is usually correlated with density fronts. As the flow is strong in these regions, nonlinearity can be important. Thus, the connections of the material geometry shown in this figure with standard fluid dynamics scaling parameters such as Rossby, internal Froude, and Richardson numbers needs to be established.

5. Discussion

We have shown here that a casual observation and subsequent analyses by Carl Eckart foresaw theoretical developments in geophysical fluid dynamics decades later. Considering the huge disparity in Reynolds numbers and energy spectra between the flow in a coffee cup and geophysical scale flows, it is remarkable that he was able to stare into the former and visualize phenomena in the latter that were not observed until satellite technology provided images of thermal patterns on the ocean surface. By applying Lagrangian methods to velocity fields generated by a data assimilating circulation model we further established that the turnstile mechanism, mediating transport between a large ocean eddy in the Gulf of Mexico and its immediate environment by finger-like invariant lobes, exists and can be traced down at least to 200m in the water column.

Of course our results strictly apply to Juggernaut during the analysis period. However, there is no reason to expect the same process would not occur through much of to Juggernaut's lifecycle as well as to other rings. The critical issue is to identify the DHT's and associated manifolds from renderings of the flow field.

The identification of the ephemeral advective transport pathways between ocean eddies and their environments that are coherent with depth has a number of potentially important ramifications. First, it has long been recognized that ocean eddies are responsible for the transport of heat and salinity from low to high latitudes. However, exactly how the eddies retain, release and redistribute these properties is not well understood. Currently operational ocean circulation models parameterize these effects as a diffusive process with eddy exchange coefficients which, in order to reflect the observed characteristics, are many orders of magnitude larger than the corresponding molecular values. However, evidence is accumulating that the eddy-induced transport requires more elaborate modelling than simply a diffusive process (e.g. [70, 71, 72, 28, 11, 29]). Instead, the exchange occurs as small, intermittent *events* resulting from interactions between the eddies and their environments via the turnstile lobes. The organizing centers for these events are often located in the nether regions between eddies and they extend well into the water column.

Second, it is important to note that the Lagrangian methods used here gave a unique material description of Juggernaut. Early theoretical models of geophysical scale eddies often appealed to bounding surfaces, such as

potential vorticity, that were approximately conserved. See [73, 74] for comprehensive reviews of these studies. However, in many observational studies of ocean eddies it is common to characterize their boundaries by sea surface temperatures and/or sea surface height anomalies determined from satellites, [75], [76]. Of course such Eulerian bounding curves are not material so they cannot provide insight into fluid exchange between eddies and their environments. Hence, in the absence of definitive observations, the theoretical models reinforced the notion that ocean eddies were exceptionally long lived and did not exchange much fluid with their environments. In contrast to this, the picture that emerges from our analysis is that even though Juggernaut was bounded by a material surface over finite time intervals, it leaks because of the turnstile mechanism operating on a time dependent interweaving material surface.

Third, if the exchange of mass between ocean eddies and their environments is significant, then present concepts on the life cycle of large ocean eddies must be modified. The standard paradigm for eddy decay is energy loss due to viscous spin down [77], Rossby wave radiation [78], or hydrodynamic instabilities [79]. Our analysis indicates that fluid was both entering and leaving Juggernaut. If the net flux of fluid is out of the eddy then this would certainly accelerate its decay.

The analysis and discussion presented here also raise new issues and questions. Perhaps the most obvious is: how common are the transport pathways identified for Juggernaut in other large eddies in the world ocean? Only in the last two decades have geophysical fluid dynamists attempted to delineate these structures. Evidence is still accumulating on the prevalence of mesoscale eddies in the world oceans and on their overall significance in transport and exchange in geophysical fluid systems (e.g. [80]).

A second issue is the potential role of vertical velocities in forming the pathways for Lagrangian transport. As noted earlier, data assimilating ocean circulation models do not yet calculate velocity as a primitive variable. Moreover, this velocity is not easily measured. This is not perceived to be a serious shortcoming for Eulerian analyses since the vertical velocity is typically believed to be several orders of magnitude smaller than the horizontal velocities. Nevertheless, any effect of its omission on the Lagrangian analyses discussed here is unknown.

Recall also that, based on the results summarized in figures 4-6, there seems to be more mass entrained into the eddy in the lower layers than in the upper layers. If this is a general property of eddies then what are the

responsible dynamical processes? Nonhydrostatic large eddy simulations and fully 3D Lagrangian transport analysis should shed considerable light on this matter.

Finally, we note that Kantha [59] observed that running CUPOM without data assimilation resulted in generation of model eddies exhibiting distinctly different behavior. These eddies are long-lived and they usually migrate across the Gulf of Mexico while retaining strong vortex signatures for many months. Such a scenario suggests little mass exchange between these model eddies and their environments which seems to be a long standing characteristic of non-data assimilating ocean circulation models (see, for example, [57, 58, 81]). In view of this fact it is appropriate to question whether the phenomena described here and in other recent studies is a peculiar artifact of the data assimilated in circulation models. This data is almost never in dynamical balance with the model at the assimilation times. As there are always data errors, assimilation routines allow for adjustments both of the new data and model dynamics. For the Gulf of Mexico the most important data source comes from altimeter data which is assimilated after being processed in a statistical database. This database acts as a low resolution filter of the primitive altimeter data, which cannot resolve the local hyperbolic hallmarks of the advective channels. Thus the enigma: are the reports of material advective pathways merely an artifact of model adjustments to data that is not in balance with model dynamics? Or, are data-assimilating models telling us something about stirring processes that Eckart envisioned over six decades ago?

Acknowledgements

This research was supported by grants N00014-07-0730, N00014-09-1-0674 and N00014-10-1-0522 from the Office of Naval Research and by the Mary A. S. Lighthipe endowment to the University of Delaware. We thank Lakshmi Kantha for his assistance with CUPOM. The authors benefitted from discussions with Bruce Lipphardt, Helga Huntley, Stephen Wiggins and Jeremy Bruch. We are also grateful to Reza Malek-Madani for his support and advice. Finally, we express our gratitude and admiration to Professor K. R. Rajagopal on the occasion of his 60th birthday. For many years we have been inspired by Raj's pursuit of excellence and innovation in science and engineering. We share with him a deep admiration for Carl Eckart.

[1] C. Eckart, An Analysis of the Stirring and Mixing Processes in Incompressible Fluids, Journal of Marine Research 7 (3) (1948) 265–275.

[2] P. Müller, C. Garrett, From stirring to mixing in a stratified ocean, Oceanography 15 (3) (2002) 12–19.

[3] S. Wiggins, The Dynamical Systems Approach to Lagrangian Transport in Oceanic Flows, Annual Review in Fluid Mechanics 37 (2005) 295–328.

[4] E. N. Lorenz, Deterministic nonperiodic flow, Journal of the Atmospheric Sciences 20 (2) (1963) 130–141.

[5] R. Samelson, S. Wiggins, Lagrangian Transport in Geophysical Jets and Waves: The Dynamical Systems Approach, Springer-Verlag, New York, 2006.

[6] J. Pedlosky, L. J. Pratt, M. A. Spall, K. R. Helfrich, Circulation around islands and ridges, J. Mar. Res. 55 (1997) 1199–1251.

[7] R. T. Pierrehumbert, H. Yang, Global chaotic mixing on isentropic surfaces, J. Atmospheric Sci. 50 (1993) 2462–2480.

[8] A. M. Rogerson, P. D. Miller, L. J. Pratt, C. K. R. T. Jones, Lagrangian motion and fluid exchange in a barotropic meandering jet, J. Phys. Oceanogr. 29 (1999) 2635–2655.

[9] K. Ngan, T. G. Shepherd, Chaotic mixing and transport in Rossby-wave critical layers, J. Fluid Mech. 334 (1997) 315–351.

[10] P. D. Miller, L. J. Pratt, K. R. Helfrich, C. K. R. T. Jones, Chaotic transport of mass and potential vorticity for an island recirculation, J. Phys. Oceanogr. 32(1) (2002) 80–102.

[11] C. Mendoza, A. M. Mancho, M.-H. Rio, The turnstile mechanism across the kuroshio current: analysis of dynamics in altimeter velocity fields, Nonlin. Processes Geophys. 17 (2010) 103–111.

[12] S. Wiggins, Normally Hyperbolic Manifolds in Dynamical Systems, Springer-Verlag, New York, 1994.

[13] I. Mezić, S. Wiggins, On the integrability and perturbation of 3-dimensional fluid-flows with symmetry, Journal of Nonlinear Science 4 (1994) 157–194.

[14] R. S. MacKay, J. D. Meiss, I. C. Percival, Stochasticity and transport in Hamiltonian systems, Phys. Rev. Lett. 52 (9) (1984) 697–700.

[15] R. S. MacKay, J. D. Meiss, I. C. Percival, Transport in Hamiltonian systems, Physica D 13 (1-2) (1984) 55–81.

[16] N. Malhotra, S. Wiggins, Geometric Structures, Lobe Dynamics, and Lagrangian Transport in Flows with Aperiodic Time-Dependence, with Applications to Rossby Wave Flow, J. Nonlinear Science 8 (1998) 401–456.

[17] J. D. Meiss, Symplectic maps, variational principles, and transport, Rev. Mod. Phys. 64 (3) (1992) 795–848.

[18] T. J. Kaper, S. Wiggins, Lobe area in adiabatic Hamiltonian systems, Physica D 51 (1-3) (1991) 205–212.

[19] V. Rom-Kedar, A. Leonard, S. Wiggins, An analytical study of transport, mixing, and chaos in an unsteady vortical flow, J. Fluid Mech. 214 (1990) 347–394.

[20] D. Beigie, A. Leonard, S. Wiggins, Invariant manifold templates for chaotic advection, Chaos, Solitons, and Fractals 4(6) (1994) 749–868.

[21] J. Ottino, The Kinematics of Mixing: Stretching, Chaos, and Transport, Cambridge University Press, Cambridge, 1989.

[22] H. Aref, M. S. El Naschie (Eds.), Chaos Applied to Fluid Mixing, Vol. 4(6) of Chaos, Solitons, and Fractals, 1994.

[23] A. Acrivos, H. Aref, J. M. Ottino (Eds.), Symposium on Fluid Mechanics of Stirring and Mixing, Vol. 3(5) of Phys. Fluids A, Part 2, 1991.

[24] A. Babiano, A. Provenzale, A. Vulpiani (Eds.), Chaotic Advection, Tracer Dynamics, and Turbulent Dispersion. Proceedings of the NATO Advanced Research Workshop and EGS Topical Workshop on Chaotic Advection, Conference Centre Sereno di Gavo, Italy, 24-28 May 1993, Vol. 76 of Physica D, 1994.

[25] S. Wiggins, The Dynamical Systems Approach to Lagrangian Transport in Oceanic Flows, Annu. Rev. Fluid Mech. 37 (2005) 295–328.

[26] C. K. R. T. Jones, S. Winkler, Invariant manifolds and Lagrangian dynamics in the ocean and atmosphere, in: Handbook of dynamical systems, North-Holland, Amsterdam, 2002, pp. 55–92.

[27] F. d'Ovidio, V. Fernández, E. H.-G. a, C. López, Mixing structures in the Mediterranean Sea from finite-size Lyapunov exponents, Geophysical Research Letters 31 (2007) L17203.

[28] A. M. Mancho, E. Hernández-García, D. Small, S. Wiggins, Lagrangian transport through an ocean front in the North-Western Mediterranean Sea, J. Phys. Oceanogr. 38 (2008) 1222–1237.

[29] M. Branicki, A. Mancho, S. Wiggins, A Lagrangian description of transport associated with a Front-Eddy interaction: Application to data from the North–Western Mediterranean Sea, Physica D (submitted for publication).

[30] P. H. Haynes, Turbulence and mixing. In *Encyclopedia of the atmospheric sciences*, Elsevier, Amsterdam, The Netherlands, 2003.

[31] E. Shuckburgh, P. Haynes, Diagnosing transport and mixing using a tracer-based coordinate system, Phys. Fluids 15(11) (2003) 3342–3357.

[32] C. Truesdell, Mechanical basis of diffusion, The Journal of Chemical Physics 37 (10) (1962) 2336 – 2344.

[33] A. Katok, B. Hasselblatt, Introduction to the Modern Theory of Dynamical Systems, Cambridge University Press, Cambridge, 1995.

[34] G. Lapeyre, Characterization of finite-time Lyapunov exponents and vectors in two-dimensional turbulence, Chaos 12(3) (2002) 688–698.

[35] B. Legras, R. Vautard, A Guide to Liapunov Vectors, in: T. Palmer (Ed.), Proceedings of the 1995 ECMWF Seminar on Predictability, 1996, pp. 143–156.

[36] M. Branicki, S. Wiggins, Finite-time lagrangian transport analysis: stable and unstable manifolds of hyperbolic trajectories and finite-time

lyapunov exponents, Nonlinear Processes in Geophysics 17 (1) (2010) 1–36.

[37] G. Haller, Lagrangian coherent structures from approximate veolcity data, Physics of Fluids 14 (6) (2002) 1851–1861.

[38] G. Haller, G. Yuan, Lagrangian coherent structures and mixing in two-dimensional turbulence, Physica D 147 (2000) 352–370.

[39] S. Shadden, F. Lekien, J. E. Marsden, Definition and properties of Lagrangian coherent structures from finite-time Lyapunov exponents in two-dimensional aperiodic flows, Physica D 212 (3-4) (2005) 271–304.

[40] K. Ide, D. Small, S. Wiggins, Distinguished hyperbolic trajectories in time dependent fluid flows: analytical and computational approach for velocity fields defined as data sets, Nonlinear Processes in Geophysics 9 (2002) 237–263.

[41] A. D. Kirwan Jr., Dynamics of critical trajectories, Progress in Oceanography 70 (2006) 448–465.

[42] S. Wiggins, Chaotic Transport in Dynamical Systems, Springer-Verlag, New York, 1992.

[43] G. Haller, A. C. Poje, Finite time transport in aperiodic flows, Physica D 119 (3-4) (1998) 352–380.

[44] N. Ju, D. Small, S. Wiggins, Existence and Computation of Hyperbolic Trajectories of Aperiodically Time-Dependent Vector Fields and Their Approximations, Int. J. Bif. Chaos 13 (2003) 1449–1457.

[45] R. S. MacKay, J. D. Meiss, I. C. Percival, Resonances in area-perserving maps, Physica D 27 (1-2) (1987) 1–20.

[46] R. S. MacKay, Transport in 3d volume-preserving flows, J. Nonlinear Sci. 4 (1984) 329–354.

[47] H. E. Lomeli, J. D. Meiss, Resonance zones and lobe volumes for volume-preserving maps, Nonlinearity 22 (2009) 1761.

[48] E. Franco, D. N. Pekarek, J. Peng, J. O. Dabiri, Geometry of unsteady fluid transport during fluid-structure interactions, Journal of Fluid Mechanics 589 (2007) 125–145.

[49] A. C. Poje, G. Haller, Geometry of cross-stream mixing in a double-gyre ocean model, J. Phys. Oceanogr. 29(8) (1999) 1649–1665.

[50] C. Coulliette, S. Wiggins, Intergyre transport in a wind-driven, quasi-geostrophic double gyre: An application of lobe dynamics, Nonlinear Processes in Geophysics 8 (2001) 69–94.

[51] B. S. Berger, M. Rokni, Lyapunov exponents and continuum kinematics, Int. J. Eng. Sci. 25 (10) (1987) 1251 – 1258.

[52] M. Branicki, S. Wiggins, An adaptive method for computing invariant manifolds in non-autonomous, three-dimensional dynamical systems, Physica D: Nonlinear Phenomena 238 (16) (2009) 1625–1657.

[53] F. Lekien, S. Shadden, J. E. Marsden, Lagrangian coherent structures in n-dimensional systems, J. Math. Phys. 48 (2007) 065404.

[54] B. A. Elliott, Anticyclonic rings in the gulf of mexico, J. Phys. Oceanogr. (12) (1982) 1579–1309.

[55] A. W. Indest, A. D. Kirwan Jr., J. K. Lewis, P. Reinersman, A synopsis of mesoscale eddies in the Gulf of Mexico, Elsevier, 1989, pp. 485–500.

[56] D. R. Johnson, J. D. Thompson, J. D. Hawkins, Circulation in the gulf of mexico from geosat altimetery during 1985-1986, J. Geophys. Res. (1992) 2201–2214.

[57] H. E. Hurlburt, J. D. Thompson, A numerical study of Loop Current intrusions and eddy shedding, J. Phys. Oceanogr. 10 (10) (1980) 1611–1651.

[58] H. E. Hurlburt, J. D. Thompson, The dynamics of Loop Current and shed eddies in a numerical model of the Gulf of Mexico, In: Hydrodynamics of Semi-enclosed Seas, Elsevier, New York, 1982, pp. 243–298.

[59] L. Kantha, J.-K. Choi, K. J. Schaudt, C. K. Cooper, A regional data-assimilative model for operational use in the Gulf of Mexico, AGU Press, 2005, pp. 165–180.

[60] B. L. Lipphardt Jr., A. C. Poje, A. D. Kirwan Jr., L. H. Kantha, M. Zweng, Death of Three Loop Current Rings, Journal of Marine Research 66 (2008) 25–60.

[61] A. D. Kirwan, M. Toner, L. Kantha, Predictability, uncertainty, and hyperbolicity in the ocean, Int. J. Eng. Sci. 41(3-5) (2003) 249–258.

[62] L. H. Kantha, C. A. Clayson, Numerical Models of Oceans and Oceanic Processes, Academic Press, 2000.

[63] G. L. Mellor, User Guide for a Three-Dimensional Primitive Equation Numerical Ocean Model (July 2002 version), Program in Atmospheric and Oceanic Sciences, Princeton University, 2002.

[64] L. H. Kantha, C. A. Clayson, An improved mixed-layer model for geophysical applications, J. Geophys. Res. 99 (C12) (1994) 25235–25266.

[65] L. H. Kantha, Development, testing and implementation of a real-time nowcast/forecast capability for the Gulf of Mexico, Monthly Kaiyo 37 (4) (2005) 239–256.

[66] J. Smagorinsky, General circulation experiments with the primitive equations, Part 1. The basic experiment, Mon. Weath. Rev. 91 (1963) 99–164.

[67] M. Toner, A. D. Kirwan Jr., L. H. Kantha, J.-K. Choi, Can general circulation models be assessed and their output enhanced with drifter data?, J. Geophys. Res.-Oceans. 106 (C9) (2001) 19563–19579.

[68] M. Toner, A. D. Kirwan, A. C. Poje, L. H. Kantha, F. E. Muller-Karger, C. K. R. T. Jones, Chlorophyll dispersal by eddy-eddy interaction in the Gulf of Mexico, J. Geophys. Res.-Oceans. 108(C4) (2003) 3105.

[69] A. M. Mancho, D. Small, S. Wiggins, Computation of Hyperbolic and their Stable and Unstable Manifolds for Oceanographic Flows Represented as Data Sets, Nonlinear Processes in Geophysics 11 (2004) 17–33.

[70] C. Wunsch, Mass and volume transport variability in an eddy-filled ocean, Nature Geosci. 1 (3) (2008) 165–168.

[71] C. Wunsch, The circulation of the ocean and its variability, Prog. Phys. Geog. 32 (4) (2008) 463–474.

[72] M. Visbeck, Power of pull, Nature 447 (2007) 383.

[73] G. Flierl, Isolated eddy models in geophysics, Ann. Rev. Fluid Mech. 19 (1987) 493–530.

[74] D. B. Olson, Rings in the ocean, Annual Review of Earth and Planetary Science 19 (1991) 283–311.

[75] R. R. Leben, Circulation in the Gulf of Mexico: Observations and Models, AGU Press, 2005, Ch. Altimeter-derived Loop Current metrics, pp. 181–201.

[76] R. R. Leben, G. H. Born, Tracking loop current eddies with satellite altimeter, Adv. Space Res. 13 (1993) 325–333.

[77] J. M. McWilliams, G. R. Flierl, Evolution of isolated, non-linear vortices, J. Phys. Oceanogr. 9 (1979) 1155–1182.

[78] G. R. Flierl, K. Haines, The decay of modons due to rossby-wave radiation, Phys. Fluids 6 (10) (1994) 3489–3497.

[79] W. K. Dewar, P. D. Killworth, On the stability of oceanic rings, J. Phys. Oceanogr. 25 (1995) 1467–1487.

[80] D. B. Chelton, M. G. Schlax, M. Samelson, R. de Szoeke, Global observations of large oceanic eddies, Geophys. Res. Lett. 34 (2007) L15606.

[81] D. E. Dietrich, C. A. Lin, A. Mestas-Nunez, D. S. Ko, A high resolution numerical study of Gulf of Mexico fronts and eddies, Meteroral. And Atmos. Phys. 64 (187-201).